Original Article

An innovative risk index based on neutrophils and macrophages can effectively predict prognosis and immunotherapy response in patients with muscle-invasive bladder cancer

Xingxing Zhang[1], Anxia Zhang[2], Lisha Hu[2], Wei Xiong[1], Panfeng Shang[1]

[1]Department of Urology, Institute of Urology, Gansu Nephro-Urological Clinical Center, Key Laboratory of Urological Diseases in Gansu Province, Lanzhou University Second Hospital, Lanzhou, China; [2]Ultrasonic Special Examination Department, Tai An TSCM Hospital, Taian, China

Contributions: (I) Conception and design: P Shang; (II) Administrative support: P Shang; (III) Provision of study materials or patients: X Zhang, W Xiong; (IV) Collection and assembly of data: X Zhang, W Xiong; (V) Data analysis and interpretation: X Zhang, A Zhang, L Hu; (VI) Manuscript writing: All authors; (VII) Final approval of manuscript: All authors.

Correspondence to: Panfeng Shang. Lanzhou University Second Hospital, Lanzhou, China. Email: shangpf@lzu.edu.cn.

Background: This study aimed to establish an innovative prognostic risk index based on tumor-infiltrating immune cells (TIICs) for patients with muscle-invasive bladder cancer (MIBC).

Methods: We used the CIBERSORT algorithm to calculate the abundance of immune cells in MIBC samples from the The Cancer Genome Atlas (TCGA) database. Univariate Cox regression analysis, least absolute shrinkage and selection operator (LASSO) regression analysis, and stepwise regression analysis were used to identify the included immune cells. Then, we constructed the risk index based on these cells through multivariate Cox regression analysis. By the risk index formula, we obtained the risk score of each patient and divided the patients into high-risk and low-risk groups. Kaplan-Meier (K-M) curve was used for survival analysis between groups. The receiver operating characteristic (ROC) curve was used to measure the prediction accuracy of the index. We validated the performance of the index in the IMvigor210 immunotherapy cohort. In addition, we established a nomogram combining the index and clinical characteristics. Finally, we performed Gene Ontology (GO) and Kyoto Encyclopedia of Genes and Genomes (KEGG) enrichment analysis of differential genes between groups.

Results: The risk index we constructed consists of three variables, including M0 macrophages, M2 macrophages, and neutrophils. K-M curve showed that the risk score had good risk stratification performance. Moreover, the risk score correlates with the patient's response to chemotherapy and immunotherapy. The nomogram has good accuracy and clinical benefit. GO and KEGG enrichment analysis revealed the tumor-promoting molecular mechanism of the index.

Conclusions: The risk index based on TIICs can facilitate individualized treatment of MIBC patients by predicting prognosis and immunotherapy response.

Keywords: Muscle-invasive bladder cancer (MIBC); risk index; macrophages; neutrophils; immunotherapy

Submitted Sep 19, 2022. Accepted for publication Feb 08, 2023. Published online Mar 17, 2023.
doi: 10.21037/tcr-22-2255
View this article at: https://dx.doi.org/10.21037/tcr-22-2255

Introduction

Bladder cancer (BLCA) is the tenth most common cancer worldwide. According to the depth of tumor invasion, BLCA is divided into non-muscle-invasive bladder cancer (NMIBC) and muscle-invasive bladder cancer (MIBC). Compared with NMIBC, MIBC has invaded at least the muscularis tissue of the bladder and is more prone to lymph node and distant metastasis. Currently, the standard treatment for MIBC is still radical cystectomy (RC) with pelvic lymph node dissection (1). However, the treatment of MIBC faces serious difficulties and challenges. In fact, MIBC patients with the same TNM stage often have

different prognostic levels, even with the same treatment regimen. In addition, although chemotherapy is an important treatment option, approximately 50% of MIBC patients are ineligible to cisplatin chemotherapy (2). Recent studies also have shown that the benefits of neoadjuvant chemotherapy are limited to only a subset of MIBC patients (2,3). Although the use of immune checkpoint blockade (ICB) therapy is a key emerging therapeutic strategy, their response rate in MIBC patients is only about 20% (4). According to statistics, the 5-year recurrence-free survival (RFS) and overall survival (OS) rates of MIBC patients after surgery were 68% and 60%, respectively, and these values were lower in patients with positive lymph nodes (5). Therefore, it is very important to develop an accurate prognostic biomarker in order to facilitate individualized treatment of MIBC patients (6).

With extensive research on the tumor microenvironment, researchers have realized the important role of tumor-infiltrating immune cells (TIICs) in tumor progression, metastasis, and treatment response (7). Indeed, the intratumoral infiltration of $CD8^+$ T cells, Th1 $CD4^+$ T cells, NK cells, and M1 macrophages (M1) is usually associated with a good prognosis, while Treg cells, Th2 $CD4^+$ T cells, MDSCs, M2 macrophages (M2), and neutrophils (Neu) are often associated with poor prognosis (5). However, since the immunosuppressive microenvironment of tumors is the result of the combined action of these different types of immune cells, a single type of immune cells is not sufficient to accurately describe the impact of the immune microenvironment on the prognosis of cancer patients. The aim of this study was to construct a TIIC-based optimal prognostic risk index to guide further treatment of MIBC patients by means of bioinformatics.

The nomogram is a reliable and convenient statistical prediction tool that combines multiple variables to predict the endpoint of interest and has been widely used in a variety of solid tumors (8). Therefore, we combined the index with other clinical characteristics to establish a nomogram associated with the prognosis of MIBC patients. In conclusion, our study developed a novel immune-related index and confirmed that the index can effectively predict the prognosis and immunotherapy response of MIBC patients. We present the following article in accordance with the TRIPOD reporting checklist (available at https://tcr.amegroups.com/article/view/10.21037/tcr-22-2255/rc).

Highlight box

Key findings

- The innovative risk index based on tumor-infiltrating neutrophils and macrophages (M0, M2) can effectively predict prognosis and immunotherapy response in patients with muscle-invasive bladder cancer (MIBC).

What is known and what is new?

- MIBC is a highly heterogeneous malignancy, and its individualized treatment still faces serious difficulties and challenges. With extensive research on the tumor microenvironment, the important role of tumor-infiltrating immune cells (TIICs) in the progression and treatment of MIBC is now widely recognized.
- However, there is still a lack of prognostic models associated with TIICs for MIBC. Therefore, a novel prognostic risk index associated with TIICs for MIBC patients was constructed for the first time in this study.

What is the implication, and what should change now?

- The risk index is an independent prognostic factor for MIBC, which correlates with the effectiveness of immunotherapy and chemotherapy and can help to improve individualized treatment of MIBC patients. In addition to macrophages, this study suggests that neutrophils are an important potential therapeutic target for MIBC. However, the present model needs further validation in a prospective cohort study.

Methods

Data acquisition and processing

The processing and normalization of research data were all achieved through the R software. First, we downloaded the clinical data and transcriptome sequencing data of 407 BLCA patients from the The Cancer Genome Atlas (TCGA) database (https://portal.gdc.cancer.gov/). According to the inclusion criteria, a total of 351 MIBC patients were included in this study for analysis. The following are the inclusion criteria in this study: (I) complete clinical information, such as age, gender, survival status, tumor node metastasis (TNM) stage, (II) T stage ≥T2, (III) histopathology belongs to urothelial carcinoma of bladder (UCB). According to the description of the "merged_sample_quality_annotations.tsv" file downloaded from the TCGA database, we excluded 7 non-UCB patients, (IV) the OS time ≥30 days. The study was conducted in accordance with the Declaration of Helsinki (as revised in 2013).

We downloaded two transcriptome matrices for TCGA-BCLA: fragments per kilobase of transcript per million mapped reads (FPKM) and Counts matrix. We used the "gencode.v38.annotation.gtf" file downloaded from the GENCODE database (https://www.gencodegenes.org/)

to complete the gene annotation of the transcriptome matrices. Repeated genes were taken to average expression values, and low-expressed genes (no expression >40 samples) were removed. Then, we downloaded the "LM22.txt" file from the CIBERSORTx database (https://cibersortx.stanford.edu/), which contains reference marker genes for 22 immune cells. We used the FPKM matrix to evaluate the abundance of TIICs through the CIBERSORT algorithm, and used the Counts matrix to analyze differential genes between groups.

Construction of immune cell-related prognostic index

The CIBERSORT algorithm is an analytical tool from the Alizadeh Lab and Newman Lab to impute gene expression profiles and provide an estimation of the abundances of member cell types in a mixed cell population, using gene expression data. We used the "cibersort.R" script to obtain the abundance of 22 TIICs in 351 MIBC tissues. Then, the MIBC samples with CIBERSORT global deconvolution P<0.2 were further included to construct the risk index. We used the "ggplot2" package to visualize the distribution of different immune cells, and used "corrplot" to visualize the correlation between immune cells. Univariate Cox regression analysis was used to identify immune cells associated with OS. Only immune cells with P<0.2 in the univariate Cox regression analysis were included in the subsequent analysis. Subsequently, through least absolute shrinkage and selection operator (LASSO) Cox regression analysis and stepwise regression analysis, we obtained the best prognostic-related immune cells. Finally, we performed multivariate Cox regression analysis on the obtained immune cells and establish the prognostic risk index:

$$\text{Risk score} = \sum_{i=1}^{n} (\beta_i * \text{Cell}_i) \quad [1]$$

among them, "n" represents the number of immune cells, "β_i" represents the regression coefficient of immune cells in the multivariate Cox regression analysis, and "Cells_i" are the abundance of immune cells.

Stratified analysis of the prognostic index

We calculated risk score for all included patients by the index and used their median as a cut-off value to classify MIBC patients into high- and low-risk groups. Kaplan-Meier (K-M) curves and log-rank tests were used for survival analysis between groups. In addition, all patients were divided into different subgroups based on different clinical characteristics. We analyzed the stratified performance of high- and low-risk patients in each subgroup by K-M curves. Moreover, we used the "timeROC" and "survival" packages to draw the receiver operating characteristic (ROC) curve of the risk score.

The prognostic index and immunotherapy response

IMvigor210 is an open-label, multicenter, single-arm phase II clinical study evaluating the efficacy and safety of PD-L1 antibody in locally advanced or metastatic urothelial carcinoma. We downloaded the IMvigor210 cohort-related data through the "IMvigor210CoreBiology" package in R software, and selected 148 patients whose histopathology was UCB as study subjects. Then, we used the same formula and method to evaluate the performance of the index. Additionally, we reveal the predictive value of the index for immunotherapy response by comparing the distribution of risk score across immunotherapy responses and immunophenotypes, respectively.

Establishment and evaluation of nomogram

We identified clinical characteristics associated with OS by K-M curves. We then performed multivariate Cox regression analysis combining these clinical characteristics and the risk score, and finally identified independent prognostic factors. Then, through the "glmnet" package and the "rms" package, these independent prognostic factors were used to establish a nomogram. We used the consistency index (C-index), calibration curve and decision curve analysis (DCA) to verify the predictive accuracy and clinical benefit of the nomogram.

Gene Ontology (GO) and Kyoto Encyclopedia of Genes and Genomes (KEGG) enrichment analysis

We used the "limma" package to analyze differential genes between groups, and selected differential genes with adj.P.Val <0.05 & abs(logFC) >1 for GO and KEGG enrichment analysis. The GO and KEGG enrichment analysis were achieved by the "clusterProfiler" package.

Moreover, these results were visualized through the "ggplot2" package, "ggrepel" package, "ggpubr" packages and "pheatmap" packages.

Statistical analysis

The correlation between TIICs was compared using Spearman's rank correlation and *t*-test to verify. The CIBERSORT algorithm was used to calculate the cell abundance of 22 TIICs. Univariate Cox regression analysis, LASSO Cox regression analysis, and stepwise regression analysis were used to identify best prognostic-related TIICs. Multivariate Cox regression analysis was used to construct the risk index and nomograms. K-M curve and log-rank test were used to compare OS rates between groups. The ROC curve was used to evaluate the discriminatory power of the prognostic index. Finally, we evaluated the accuracy and clinical benefits of the nomogram through the C-index, calibration curve and DCA. All statistical calculations in this study were done in R-4.1.0 software.

Results

TIICs

We obtained the abundance of 22 TIICs in MIBC samples by the CIBERSORT algorithm. According to the standard of CIBERSORT global deconvolution P<0.2, 269 MIBC patients were selected to construct the risk index. In MIBC tissue, M0, M2 and $CD8^+$ T cells were the most infiltrating immune cells (*Figure 1A-1C*). Resting mast cells was negatively correlated with activated mast cells (r=–0.67), activated NK cells was negatively correlated with resting NK cells (r=–0.46), M0 was negatively correlated with monocytes and $CD8^+$ T cells (r=–0.52 and r=–0.46), $CD8^+$ T cells was positively correlated with activated memory $CD4^+$T cells (r=0.61), and plasma cells was positively correlated with naive B cells (r=0.52) (*Figure 1D*).

TIICs-based risk index

First, we identified TIICs associated with OS by univariate Cox regression analysis (P<0.2). They all include: plasma cells, $CD8^+$ T cells, activated memory $CD4^+$T cells, helper follicular T cells, M0, M2, activated mast cells, and Neu (*Table 1*). Through the LASSO regression analysis, we excluded $CD8^+$ T cells and helper follicular T cells, which have multicollinearity problems (*Figure 2A,2B*). Finally, by stepwise regression analysis, M0, M2 and Neu were identified as the included variables for the best prognostic model. Then, the risk index using these TIICs as a variable was constructed by multivariate Cox regression analysis. The formula was as follows: Risk score = 1.63 × M0 + 2.33 × M2 + 11.6 × Neutrophils.

Stratification performance of the risk index

We used this formula to calculate the risk score for each included patient. Then, we divided the patients into high-risk group and low-risk group with the median of the risk score (0.573). K-M curves showed that patients in the low-risk group had a significantly higher OS rate compared with the high-risk group (P<0.0001) (*Figure 2C*). The area under curve (AUC) of the risk score was 0.686 at year 1, 0.667 at year 2, and 0.630 at year 3 (*Figure 2D*). Moreover, the risk score was well stratified in each of the following subgroups of patients [including T stage (T3), T stage (T4), N stage (N0), N stage (N1/2/3), M0, TNM (III), TNM (IV), gender (male), pharmaceutical treatment (yes)/(no), and age (>65 years)/(≤65 years)]. However, it performed poorly in the subgroups of T stage (T2), TNM stage (II), and gender (female) (*Figure 3*). Of note, we accidentally discovered that patients with distant metastases were all classified into the high-risk group. This made it impossible for us to do a stratification analysis of distant metastasis (M1).

Correlation of risk index with immunotherapy and chemotherapy

In the IMvigor210 cohort, K-M survival curves also indicated that patients in the low-risk group had significantly higher OS rates than those in the high-risk group (P=0.0017, *Figure 4A*). The AUC of the risk score was 0.629 months 12, 0.693 months 18, and 0.717 months 20 (*Figure 4B*). Patients who did not respond to anti-PD-L1 immunotherapy had significantly higher risk score than those who responded (P=0.038, *Figure 4C*). In addition, the risk score was significantly different among the three tumor immunophenotypes (risk score: inflamed < excluded < desert, P=0.0065, *Figure 4D*). Moreover, boxplot showed that the risk score was significantly higher in the cisplatin-treated patient sample than in the untreated patients (P=0.012, *Figure 4E*). K-M survival curves showed that in the "neoadjuvant chemotherapy (NAC)" (P=0.0062, *Figure 4F*), "adjuvant chemotherapy (AC)" (P=0.00027, *Figure 4G*) and "Received_platinum_no" subgroups (P=0.036, *Figure 4H*), patients in the low-risk group had significantly

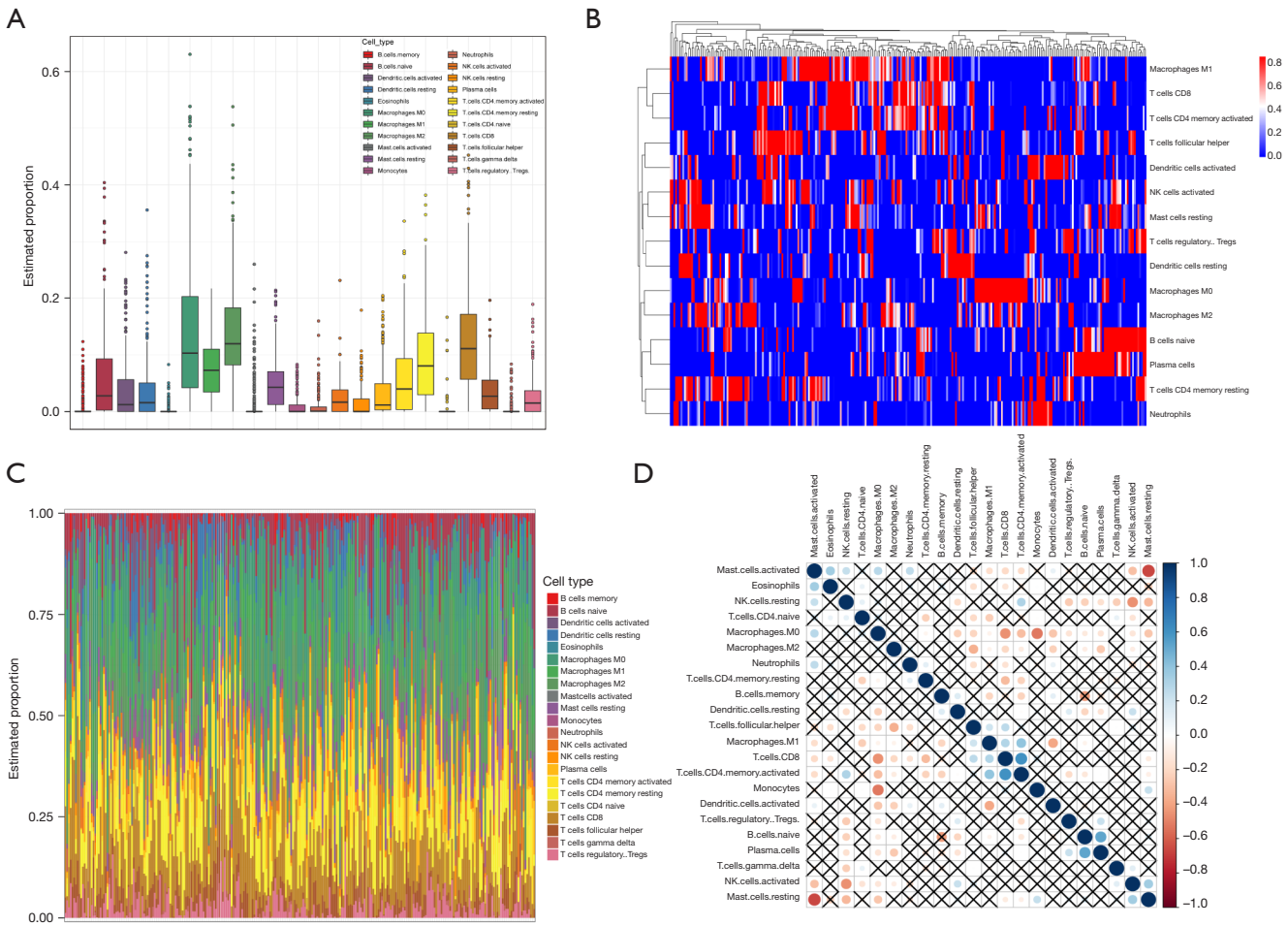

Figure 1 Distribution and correlation of TIICs in MIBC samples. (A) Box plot shows the overall distribution of the 22 TIICs across all MIBC samples. (B,C) Heatmaps and bar plot present the distribution of TIICs within each sample. (D) The correlation matrix of TIICs presents the correlation between immune cells. Red balls represent negative correlations, blue balls positive correlations. The correlation coefficient of the test level P>0.05 is represented by "×". TIICs, tumor-infiltrating immune cells; MIBC, muscle-invasive bladder cancer.

higher OS rates than those in the high-risk group.

Nomogram based on the risk index

The K-M curve indicated that T stage, N stage, TNM stage, age, and pharmaceutical treatment were all clinical characteristics associated with OS (P<0.05, Figure S1). Considering the correlation between Tumor stage, N stage and TNM stage, we only kept the former for the next analysis. Because there were 28 patients whose pharmaceutical treatment was in the "not reported" status, we selected the data of the remaining 323 patients to construct a nomogram. Then, the results of multivariate Cox regression analysis of the risk score and prognosis-related clinical characteristics showed that the risk score, T stage, N stage, age, and pharmaceutical treatment were all independent prognostic factors (Figure S2), and they were used to establish a nomogram (*Figure 5A*). The C-index of the nomogram was 0.719 [95% confidence interval (CI): 0.696–0.742]. Calibration curves for 1, 3, and 5 years show good accuracy for the nomogram (*Figure 5B-5D*). Furthermore, DCA showed better clinical benefit of nomogram compared to the TNM staging system (*Figure 5E-5G*).

GO and KEGG function enrichment analysis

We obtained a total of 194 differential genes between

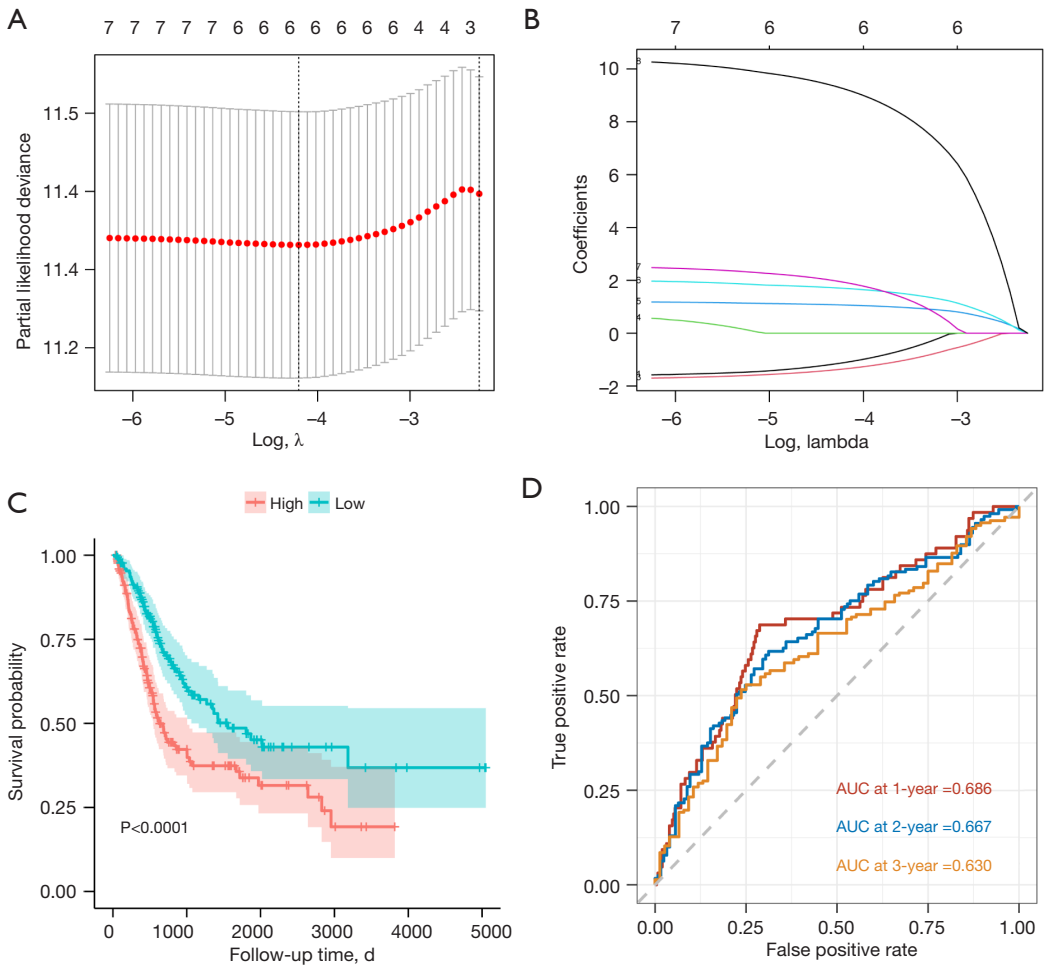

Figure 2 Construction and evaluation of risk index. (A,B) Through the LASSO Cox regression, we excluded CD8+ T cells and helper follicular T cells, which have multicollinearity problems. (C) K-M curve indicted that high-risk scores were associated with poor prognosis (P<0.0001). (D) ROC curve for predicting prognosis by risk score. The AUC of the risk score was 0.686 at year 1, 0.667 at year 2, and 0.630 at year 3. AUC, area under curve; LASSO, least absolute shrinkage and selection operator; K-M, Kaplan-Meier; ROC, receiver operating characteristic.

the two groups in the TCGA-MIBC dataset, including 117 up-regulated genes and 77 down-regulated genes (Table S1). Volcano plot and heatmap were used to visualize the results (Figure S3). GO and pathway analysis showed that the up-regulated genes were mainly enriched in the processes of extracellular matrix organization, extracellular structure organization, external encapsulating structure organization, skeletal system development, wound healing and skin development (*Figure 6A-6C*). Additionally, the results of KEGG enrichment analysis showed that up-regulated genes were mainly enriched in protein digestion and absorption, IL-17 signaling pathway, extracellular matrix (ECM)-receptor interaction and PI3K-Akt signaling pathway, while down-regulated genes were mainly enriched in arachidonic acid metabolism, pancreatic secretion, aldosterone-regulated sodium reabsorption, alpha-linolenic acid metabolism and linoleic acid metabolism (*Figure 6D*).

Discussion

Tumor microenvironment (TME) usually includes many different immune cell subgroups with anti-tumor or tumor-promoting activities. A growing body of evidence shows that the interaction between TIICs and cancer cells affects the progression of cancer and the response to immunotherapy drugs. However, since the immunosuppressive microenvironment of tumors is the result of the combined action of different types of immune cells, a single type of

Table 1 Univariate Cox regression analysis for 22 TIICs in the TCGA-MIBC dataset

TIICs	HR (95% CI for HR)	P value
B.cells.naive	0.46 (0.055–3.8)	0.47
B.cells.memory	0.0032 (2.6e-07–39)	0.23
Plasma.cells	0.045 (0.00073–2.7)	0.14
T.cells.CD8	0.086 (0.0099–0.74)	0.025
T.cells.CD4.naive	580 (0.017–2e+07)	0.23
T.cells.CD4.memory.resting	1.1 (0.11–11)	0.93
T.cells.CD4.memory.activated	0.038 (0.0019–0.77)	0.033
T.cells.follicular.helper	0.026 (0.00014–4.8)	0.17
T.cells.regulatory.Tregs.	0.071 (0.00026–20)	0.36
T.cells.gamma.delta	0.00022 (2.6e-11–1,800)	0.3
NK.cells.resting	0.0076 (3.4e-06–17)	0.21
NK.cells.activated	0.029 (5.6e-05–15)	0.27
Monocytes	7 (0.00013–370,000)	0.73
Macrophages.M0	5.7 (1.6–20)	0.0061
Macrophages.M1	0.65 (0.021–20)	0.81
Macrophages.M2	11 (1.7–69)	0.012
Dendritic.cells.resting	0.46 (0.023–9.2)	0.61
Dendritic.cells.activated	0.58 (0.025–13)	0.73
Mast.cells.resting	7.3 (0.22–240)	0.27
Mast.cells.activated	210 (1.8–25,000)	0.028
Eosinophils	8.3 (8.3e-07–8.3e+07)	0.8
Neutrophils	74,000 (35–1.5e+08)	0.004

TIICs, tumor-infiltrating immune cells; TCGA-MIBC, The Cancer Genome Atlas-muscle invasive bladder cancer; HR, hazard ratio; CI, confidence interval.

immune cells is not sufficient to accurately describe the impact of the immune microenvironment on the prognosis of cancer patients. Therefore, this study is the first to construct a prognostic risk index based on TIICs for MIBC patients, aiming to improve the prediction level of prognosis and immunotherapy response, and promote individualized treatment of MIBC patients.

The risk index formula consists of three variables, including M0, M2, and Neu. Multivariate Cox regression analysis indicated that the index was an independent prognostic factor for MIBC patients. In fact, this may be because high infiltration levels of both macrophages (9-12) and neutrophils (13-16) are associated with tumor progression and poor prognosis. TME can promote the recruitment and polarization of macrophages in different ways. Although macrophages can be polarized into a series of phenotypes, the most common types are "M1" and "M2". Both M1 and M2 are involved in the progression of tumors, but M1 plays a role in suppressing tumors through acute inflammation, while M2 promotes chronic inflammation and leads to immune suppression and tumor growth. At present, hundreds of cancer clinical trials targeting tumor-associated macrophages (TAMs) have been registered, including BLCA clinical trials (11). The main molecular mechanisms of these macrophage-targeted drugs include: inhibition of macrophage recruitment, depletion of TAMs, reprograming of TAMs, and activation of antitumor function of TAMs. Similar to TAMs, tumor-associated neutrophils (TANs) can also be polarized into anti-tumor (N1) or pro-tumor (N2) phenotypes. Interestingly, like TAMs, TANs often exhibit antitumor activity in the early stages of cancer, and gradually shift to pro-tumor activity during tumor progression (16-18). In addition, the latest research shows that neutrophils play a key role in the process of tumor metastasis (14). Fortunately, the efficacy of neutrophil-targeted drugs such as CXCL8 and CXCR1 blockers in solid tumors has entered clinical evaluation. Therefore, the risk index combines the predictive power of macrophages and neutrophils, which proves the reliability of the index.

In the stratification analysis, the risk score performed well in the subgroups of T stage (T3), T stage (T4), N stage (N0), N stage (N1/2/3), M0, TNM stage (III), TNM stage (IV), gender (male), pharmaceutical treatment (yes)/(no) and age (>65 years)/(≤65 years). However, they performed poorly in the subgroups of T2, TNM stage (II), and gender (female). The reasons for the poor performance of risk stratification in female patients may be related to the smaller sample size of female patients and more factors affecting the prognosis of female patients (19,20). As mentioned above, macrophages and neutrophils have anti-tumor activity in the early stages of tumors, and gradually transit to the tumor-promoting activities during tumor progression. This may account for the poor performance of the risk score in risk stratification in patients with earlier MIBC. The above results suggest that risk stratification of MIBC patients according to the risk score can help clinicians make decisions and improve patient outcomes. For example, good stratification performance in pharmaceutical treatment subgroup suggests that patients with lower risk score are more likely to benefit from the treatment.

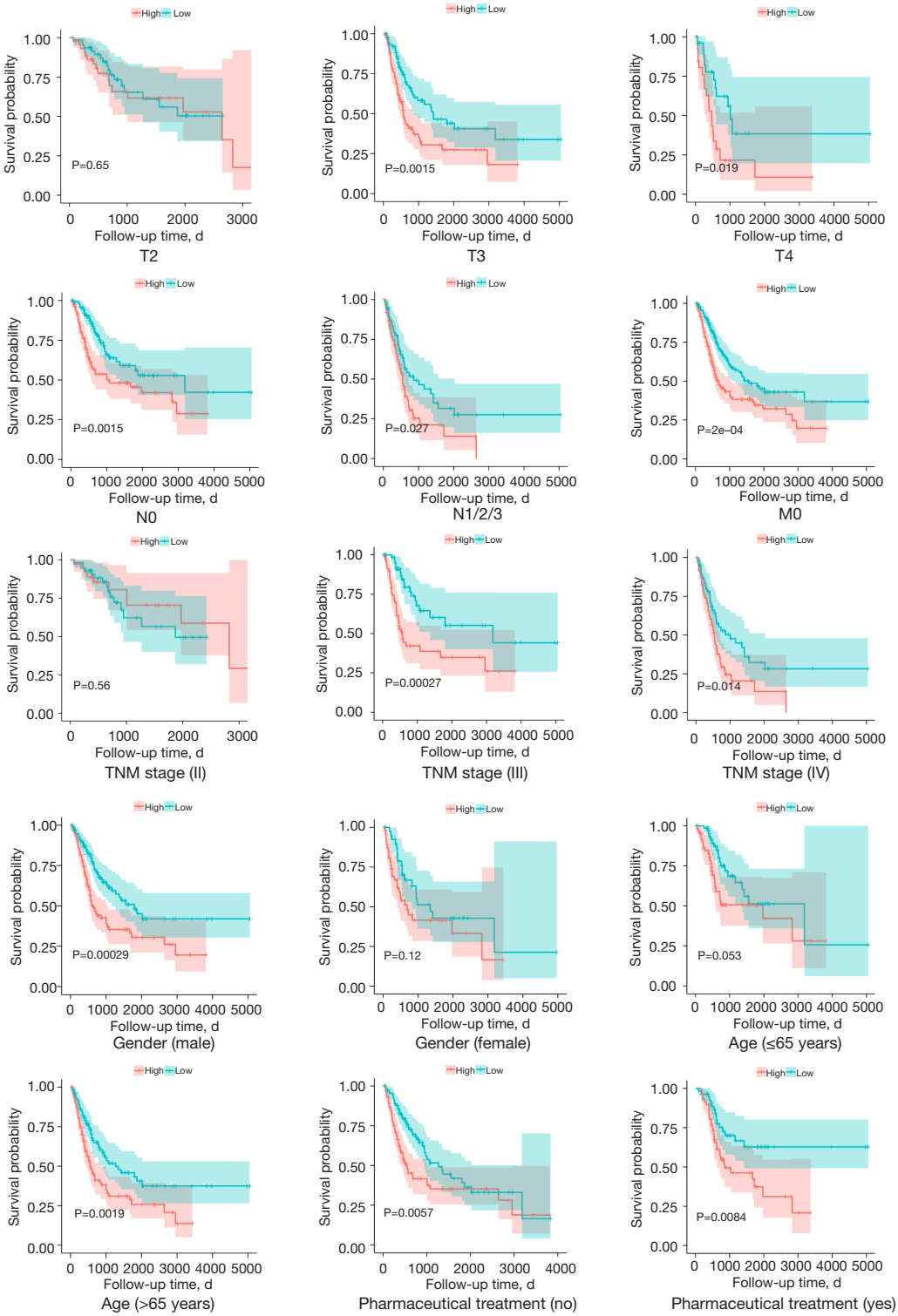

Figure 3 Stratified analysis of the risk score in different subgroups. The risk score performed well in the subgroups of T stage (T3), T stage (T4), N stage (N0), N stage (N1/2/3), M0, TNM stage (III), TNM stage (IV), gender (male), pharmaceutical treatment (yes)/(no) and age (>65 years)/(≤65 years). However, they performed poorly in the subgroups of T2, TNM stage (II), and gender (female). TNM, tumor node metastasis.

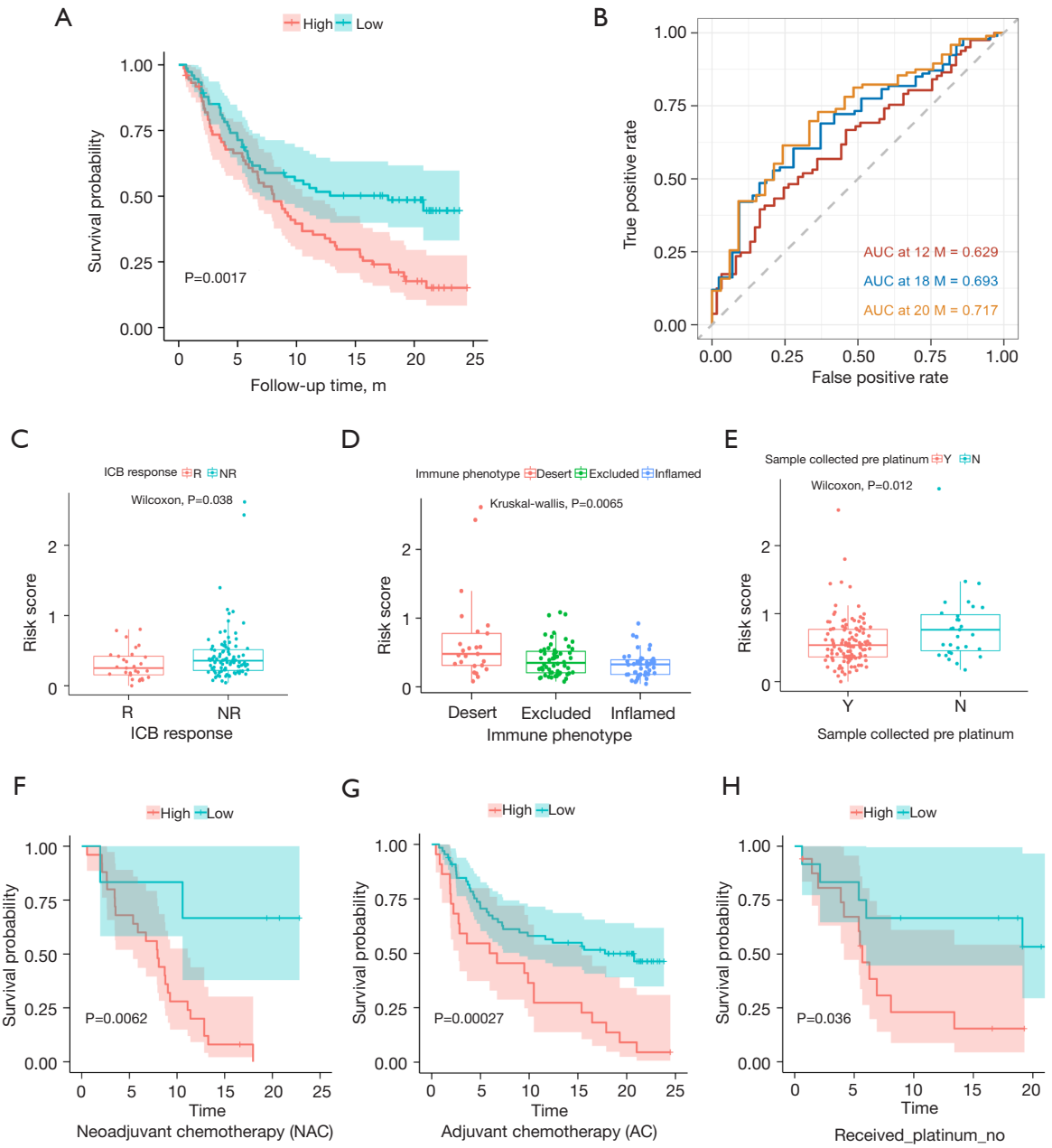

Figure 4 Performance of the risk score in the IMvigor210 cohort. (A) The K-M curve indicated that patients with low-risk score had a significantly higher OS rate than those with high score (P=0.0017). (B) AUC for the risk score was 0.629 months 12, 0.693 months 18 and 0.717 months 20. (C) The risk score value of patients who responded to anti-PD-L1 immunotherapy was significantly lower than that of patients who did not respond (P=0.038). (D) The risk score values were significantly different among the three tumor immunophenotypes (inflamed < excluded < desert, P=0.0065). (E) Box plot showed that the risk score was significantly higher in the cisplatin-treated patient sample than in the untreated patients (P=0.012). (F-H) K-M survival curves showed that in the "NAC" (P=0.0062), "AC" (P=0.00027) and "Received_platinum_no" subgroups (P=0.036), patients in the low-risk group had significantly higher OS rates than those in the high-risk group. AUC, area under curve; K-M, Kaplan-Meier; OS, overall survival; NAC, neoadjuvant chemotherapy; AC, adjuvant chemotherapy.

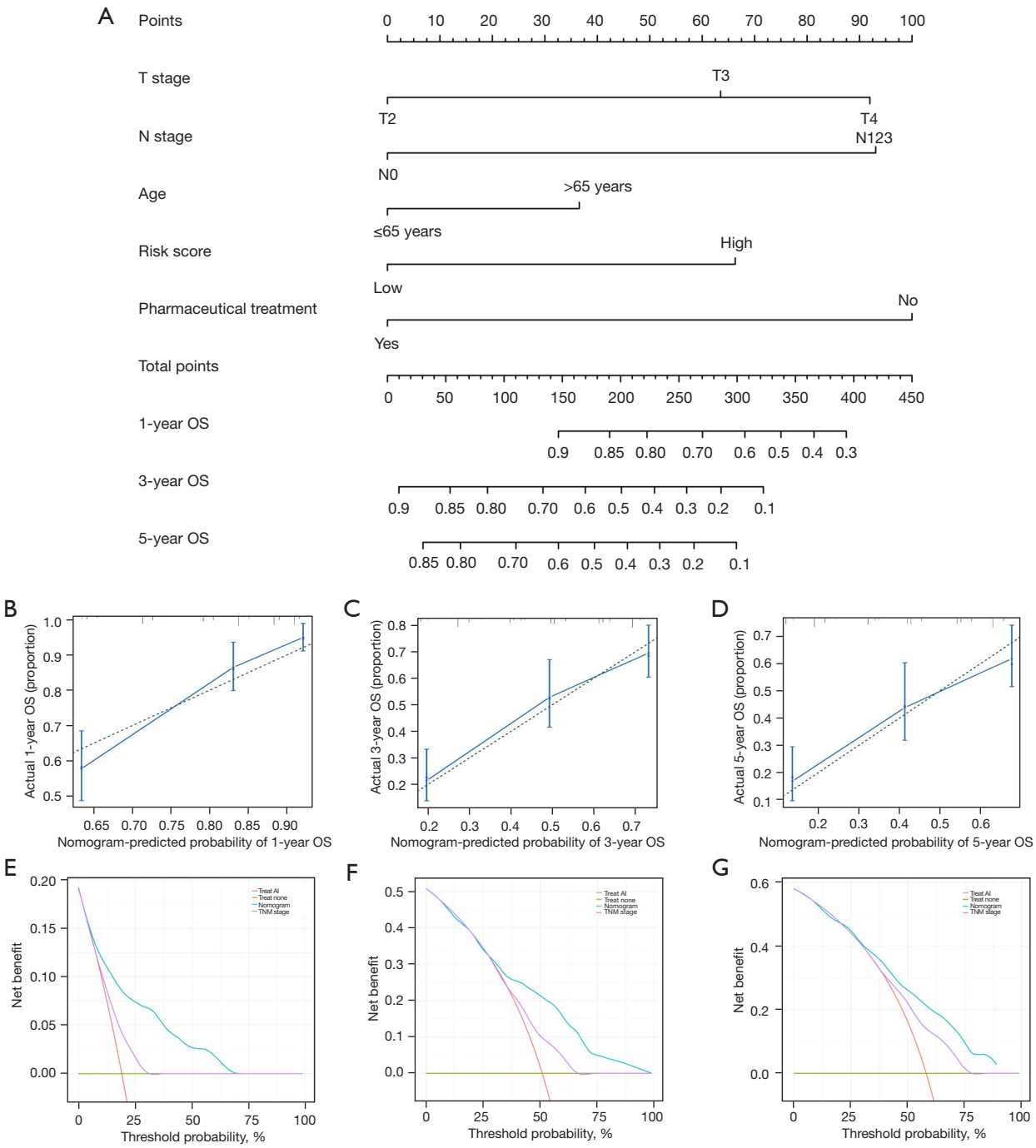

Figure 5 Nomogram plotting and evaluation. (A) Nomogram for the prediction of OS at 1, 3 and 5 years. (B-D) The calibration curve demonstrated agreement between the predictive and observed outcomes for OS at 1, 3 and 5 years. (E-G) DCA showed better clinical benefit of nomogram compared to the TNM staging system. OS, overall survival; AI, artificial intelligence; DCA, decision curve analysis; TNM, tumor node metastasis.

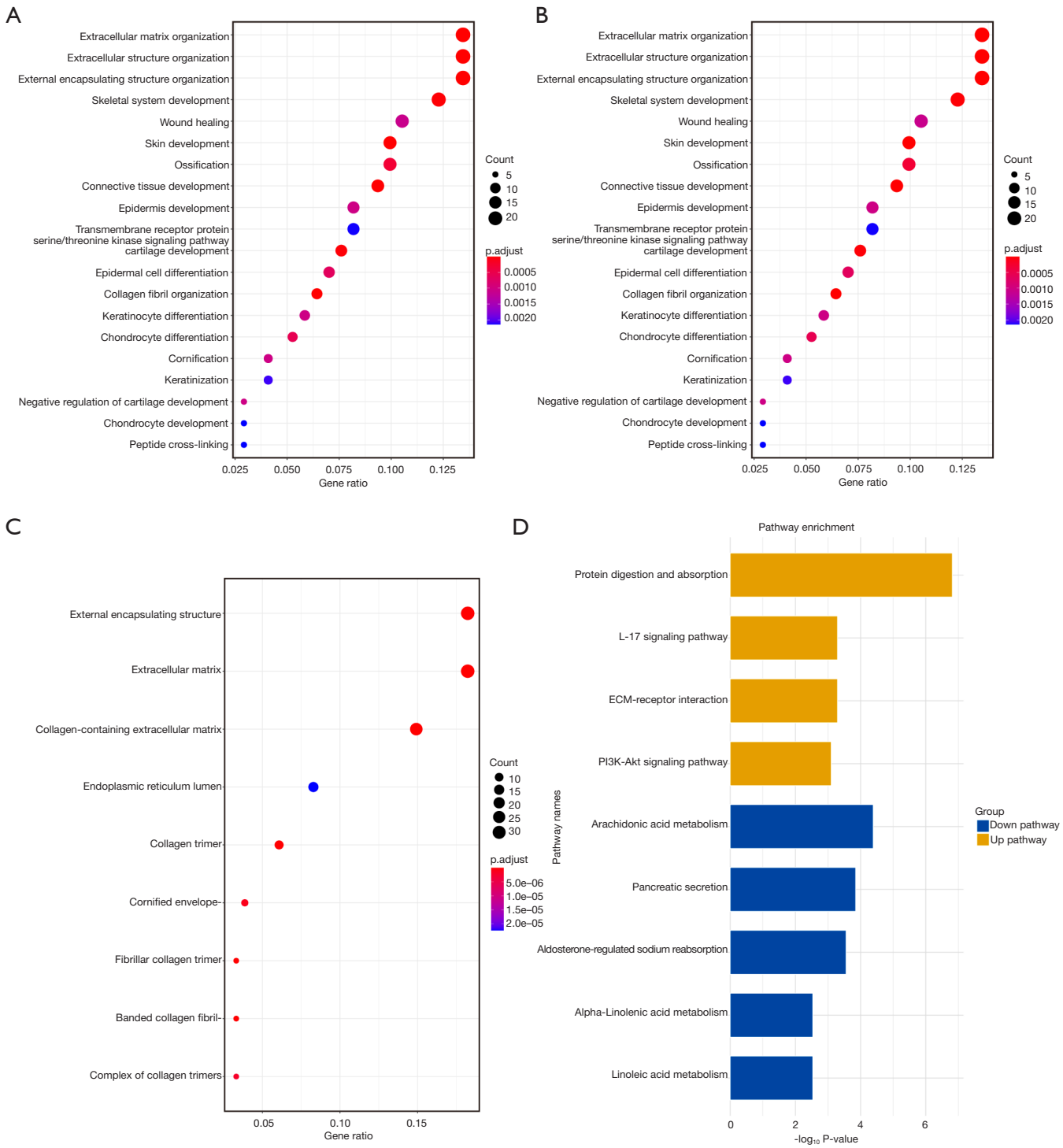

Figure 6 GO and KEGG functional enrichment analysis of the differential genes. (A) The GO term, BP of the difference genes. (B) The GO term, MF of the difference genes. (C) The GO term, CC of the difference genes. (D) KEGG enrichment analysis of the difference genes. GO, Gene Ontology; KEGG, Kyoto Encyclopedia of Genes and Genomes; BP, biological processes; MF, molecular functions; CC, cell components.

With the in-depth study of TME, anti-tumor immunotherapy has been successfully developed and applied in patients with refractory or metastatic cancer. Among them, ICB therapy targeting $CD8^+$ T cells has achieved significant clinical effects in some cancer patients (21). But in fact, the overall response rate of ICB therapy in MIBC patients is only about 20%. Studies have shown that the tumor immunosuppressive microenvironment can render ICB therapy ineffective by limiting the infiltration and activation of T effector cells (22,23). Therefore, we analyzed the association of the risk score with immunotherapy response through the IMvigor210 cohort. First, we confirmed that the risk score was associated with OS in these patients by K-M curves. Moreover, the ROC curve shows that the index has good discrimination as a predictor. Then, we found that the risk score were significantly different among the three immunophenotypes in MIBC (risk scores: inflamed < excluded < desert, P=0.0065). Finally, the risk score of patients who responded to PD-L1 antibody was significantly lower than that of patients who did not respond (P=0.038). Together, these results suggest that the risk score correlates with infiltration and activation of T effector cells and thus serves as a predictor of ICB treatment response.

Because the nomogram can predict a patient's prognosis by combining multiple variables, it has shown higher predictive accuracy than the TNM staging system. In order to further improve the accuracy of prognosis prediction of MIBC patients, we combined TIICs-related index and clinical characteristics to establish a nomogram. The results of C-index and clinical decision curve show that the nomogram has good accuracy and calibration. In addition, the 1-, 3-, and 5-year DCA results showed that the nomogram we established had a higher clinical benefit compared with the TNM staging system.

Finally, the GO and KEGG enrichment analysis of the differential genes between high-risk group and low-risk group showed that up-regulated genes were enriched in protein digestion and absorption, IL-17 signaling pathway, ECM-receptor interaction, and PI3K-Akt signaling pathway. Down-regulated genes were enriched in the pathways of arachidonic acid metabolism, pancreatic secretion, aldosterone-regulated sodium reabsorption, alpha-linolenic acid metabolism, and linoleic acid metabolism. These pathways may be associated with tumor-promoting mechanisms of macrophages and neutrophils. It was found that IL-17 produced by γδT cells can promote neutrophil recruitment and polarization by regulating the release of granulocyto-colony-stimulating-factor (G-CSF) (24). Moreover, the production of IL-17 is induced by IL-1β secreted by TAMs (25). It is worth mentioning that in the cellular component (CC) analysis, the genes for collagen synthesis were the most expressed gene among the differential genes. In fact, recent studies found that collagen secreted by TAMs can activate the PI3K-Akt signaling pathway through integrin α2β1 to promote the progress of BLCA (11,26). In this study, down-regulated genes are mainly enriched in lipid metabolism pathways, which may lead to a high lipid state in the TME (27). Of note, the high lipid state in the TME can activate the immunosuppressive phenotype of macrophages and neutrophils, thereby promoting the progress of MIBC (28-30).

This study has some limitations. First, this study is a retrospective analysis of publicly available data, which leads to inevitable selection biases. Second, because our study is based on bioinformatic analysis, prospective clinical studies are needed to validate our findings. Third, we failed to incorporate other important prognostic factors in MIBC patients when establishing the nomogram. In future studies, we will try to incorporate more prognostic factors to improve the predictive effect of this nomogram.

Conclusions

In this study, we constructed a prognostic risk index based on TIICs for patients with MIBC. The index is an independent prognostic factor for MIBC patients and has good stratification performance. Furthermore, we demonstrated that the index is associated with immunotherapy response and has potential value in predicting immunotherapy efficacy. In conclusion, we developed a novel prognostic biomarker for MIBC patients that could facilitate individualized treatment of MIBC patients.

Acknowledgments

Funding: This work was supported by the Key Research and Development (R&D) projects of Gansu Province (Grant No. 17YF1FA126); Lanzhou Science and Technology Bureau Medical and Health Project (Grant No. 2021-90); Special fund project for doctoral training program of Lanzhou University Second Hospital (Grant No.YJS-BD-25); and CuiYing Science and Technology Innovation plan project of Lanzhou University Second Hospital (Grant No. CY2017-BJ05).

Footnote

Reporting Checklist: The authors have completed the TRIPOD checklist. Available at https://tcr.amegroups.com/article/view/10.21037/tcr-22-2255/rc

Conflicts of Interest: All authors have completed the ICMJE uniform disclosure form (available at https://tcr.amegroups.com/article/view/10.21037/tcr-22-2255/coif). The authors have no conflicts of interest to declare.

Ethical Statement: The authors are accountable for all aspects of the work in ensuring that questions related to the accuracy or integrity of any part of the work are appropriately investigated and resolved. The study was conducted in accordance with the Declaration of Helsinki (as revised in 2013).

References

1. Witjes JA, Bruins HM, Cathomas R, et al. European Association of Urology Guidelines on Muscle-invasive and Metastatic Bladder Cancer: Summary of the 2020 Guidelines. Eur Urol 2021;79:82-104.
2. Patel VG, Oh WK, Galsky MD. Treatment of muscle-invasive and advanced bladder cancer in 2020. CA Cancer J Clin 2020;70:404-23.
3. Ruiz de Porras V, Pardo JC, Etxaniz O, et al. Neoadjuvant therapy for muscle-invasive bladder cancer: Current clinical scenario, future perspectives, and unsolved questions. Crit Rev Oncol Hematol 2022;178:103795.
4. Oh DY, Kwek SS, Raju SS, et al. Intratumoral CD4(+) T Cells Mediate Anti-tumor Cytotoxicity in Human Bladder Cancer. Cell 2020;181:1612-25.e13.
5. Schneider AK, Chevalier MF, Derré L. The multifaceted immune regulation of bladder cancer. Nat Rev Urol 2019;16:613-30.
6. Cathomas R, Lorch A, Bruins HM, et al. The 2021 Updated European Association of Urology Guidelines on Metastatic Urothelial Carcinoma. Eur Urol 2022;81:95-103.
7. Tran L, Xiao JF, Agarwal N, et al. Advances in bladder cancer biology and therapy. Nat Rev Cancer 2021;21:104-21.
8. Yang H, Zhang R, Zhang R, et al. Nomogram for distant metastasis-free survival in patients with locoregionally advanced nasopharyngeal carcinoma. Strahlenther Onkol 2022;198:828-37.
9. Zhang X, Bai W, Hu L, et al. The pleiotropic mode and molecular mechanism of macrophages in promoting tumor progression and metastasis. Clin Transl Oncol 2023;25:91-104.
10. Cassetta L, Pollard JW. Targeting macrophages: therapeutic approaches in cancer. Nat Rev Drug Discov 2018;17:887-904.
11. Leblond MM, Zdimerova H, Desponds E, et al. Tumor-Associated Macrophages in Bladder Cancer: Biological Role, Impact on Therapeutic Response and Perspectives for Immunotherapy. Cancers (Basel) 2021;13:4712.
12. Christofides A, Strauss L, Yeo A, et al. The complex role of tumor-infiltrating macrophages. Nat Immunol 2022;23:1148-56.
13. Németh T, Sperandio M, Mócsai A. Neutrophils as emerging therapeutic targets. Nat Rev Drug Discov 2020;19:253-75.
14. Güç E, Pollard JW. Redefining macrophage and neutrophil biology in the metastatic cascade. Immunity 2021;54:885-902.
15. Coffelt SB, Wellenstein MD, de Visser KE. Neutrophils in cancer: neutral no more. Nat Rev Cancer 2016;16:431-46.
16. Shaul ME, Fridlender ZG. Tumour-associated neutrophils in patients with cancer. Nat Rev Clin Oncol 2019;16:601-20.
17. Ng LG, Ostuni R, Hidalgo A. Heterogeneity of neutrophils. Nat Rev Immunol 2019;19:255-65.
18. Jaillon S, Ponzetta A, Di Mitri D, et al. Neutrophil diversity and plasticity in tumour progression and therapy. Nat Rev Cancer 2020;20:485-503.
19. Dobruch J, Daneshmand S, Fisch M, et al. Gender and Bladder Cancer: A Collaborative Review of Etiology, Biology, and Outcomes. Eur Urol 2016;69:300-10.
20. Radkiewicz C, Edgren G, Johansson ALV, et al. Sex Differences in Urothelial Bladder Cancer Survival. Clin Genitourin Cancer 2020;18:26-34.e6.
21. Ribas A, Wolchok JD. Cancer immunotherapy using checkpoint blockade. Science 2018;359:1350-5.
22. Kersten K, Hu KH, Combes AJ, et al. Spatiotemporal co-

dependency between macrophages and exhausted CD8(+) T cells in cancer. Cancer Cell 2022;40:624-38.e9.
23. Zhang X, Du Y, Xiong W, et al. Combined single-cell RNA-seq and bulk RNA-seq to analyze the expression and role of TREM2 in bladder cancer. Med Oncol 2022;40:23.
24. Coffelt SB, Kersten K, Doornebal CW, et al. IL-17-producing γδ T cells and neutrophils conspire to promote breast cancer metastasis. Nature 2015;522:345-8.
25. Kersten K, Coffelt SB, Hoogstraat M, et al. Mammary tumor-derived CCL2 enhances pro-metastatic systemic inflammation through upregulation of IL1β in tumor-associated macrophages. Oncoimmunology 2017;6:e1334744.
26. Qiu S, Deng L, Liao X, et al. Tumor-associated macrophages promote bladder tumor growth through PI3K/AKT signal induced by collagen. Cancer Sci 2019;110:2110-8.
27. Masetti M, Carriero R, Portale F, et al. Lipid-loaded tumor-associated macrophages sustain tumor growth and invasiveness in prostate cancer. J Exp Med 2022;219:e20210564.
28. Veglia F, Tyurin VA, Blasi M, et al. Fatty acid transport protein 2 reprograms neutrophils in cancer. Nature 2019;569:73-8.
29. Al-Khami AA, Zheng L, Del Valle L, et al. Exogenous lipid uptake induces metabolic and functional reprogramming of tumor-associated myeloid-derived suppressor cells. Oncoimmunology 2017;6:e1344804.
30. Di Conza G, Tsai CH, Gallart-Ayala H, et al. Tumor-induced reshuffling of lipid composition on the endoplasmic reticulum membrane sustains macrophage survival and pro-tumorigenic activity. Nat Immunol 2021;22:1403-15.

Cite this article as: Zhang X, Zhang A, Hu L, Xiong W, Shang P. An innovative risk index based on neutrophils and macrophages can effectively predict prognosis and immunotherapy response in patients with muscle-invasive bladder cancer. Transl Cancer Res 2023;12(3):536-549. doi: 10.21037/tcr-22-2255

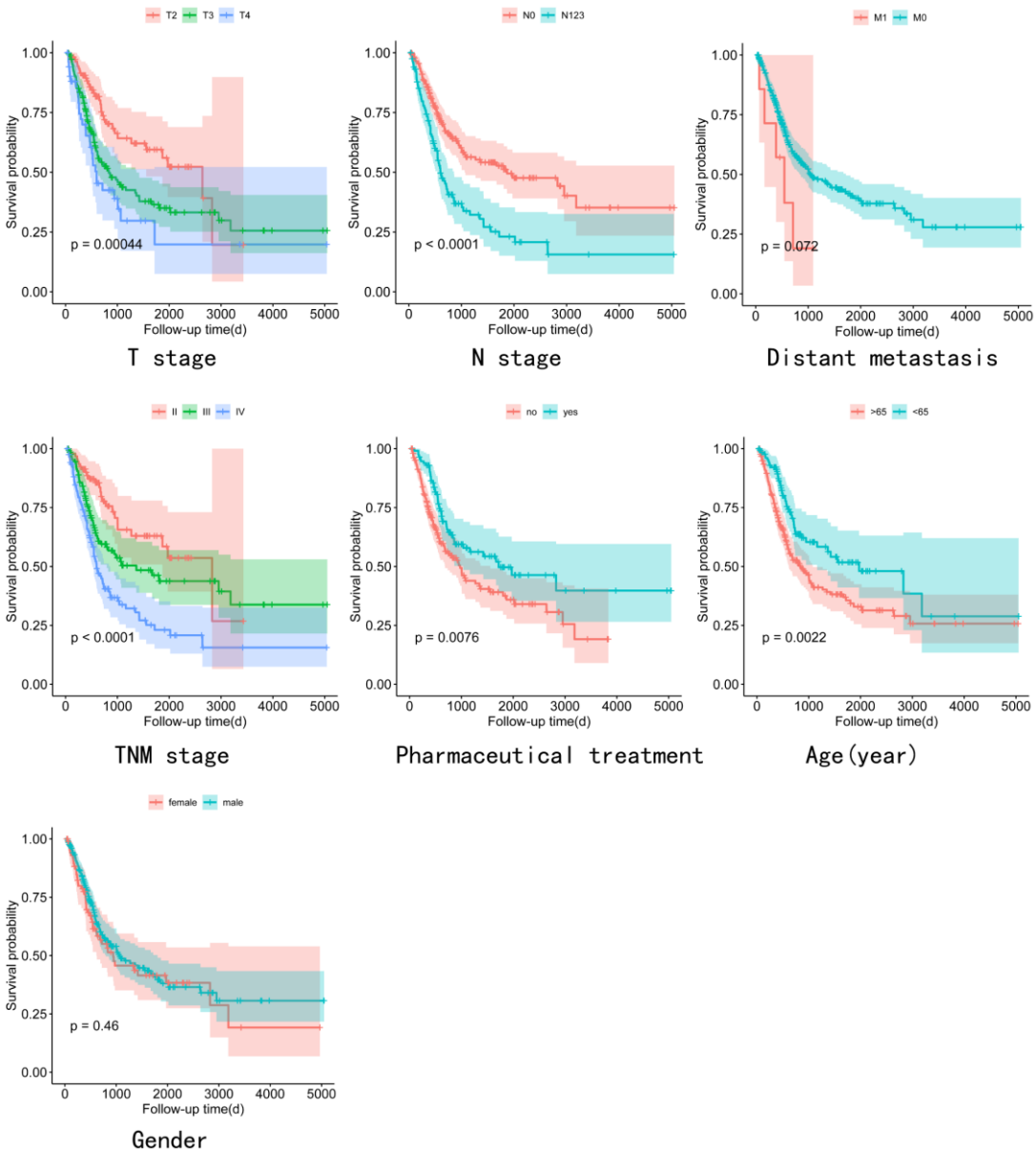

Figure S1 Kaplan-Meier curve analysis of clinical characteristics. Kaplan-Meier curve showed that T stage, N stage, TNM stage, age and pharmaceutical treatment were associated with the prognosis of MIBC patients. TNM, tumor node metastasis; MIBC, muscle-invasive bladder cancer.

https://dx.doi.org/10.21037/tcr-22-2255

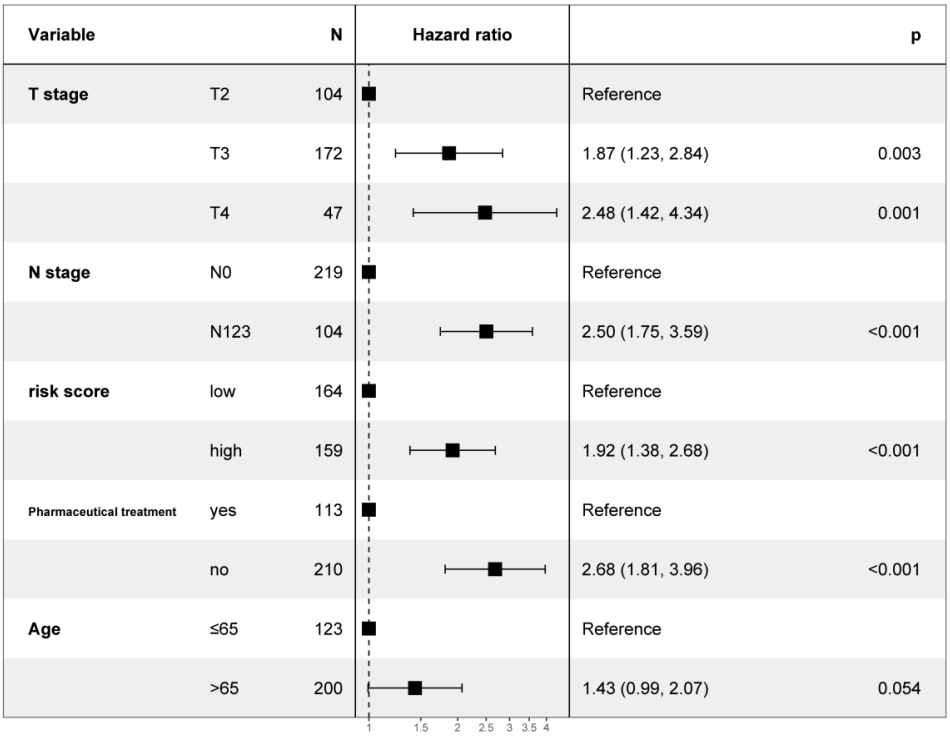

Figure S2 The results of multivariate Cox regression analysis of the risk score and prognosis-related clinical characteristics showed that the risk score, T stage, N stage, age, and pharmaceutical treatment were all independent prognostic factors.

https://dx.doi.org/10.21037/tcr-22-2255

Table S1 List of the 194 differential genes between groups

Gene	logFC	AveExpr	t	P.Value	adj.P.Val	B	Change
IGLON5	1.353827	-1.756110	7.396219	1.03E-12	2.06E-08	17.850640	UP
HSH2D	-1.037600	3.568963	-6.986460	1.41E-11	1.41E-07	15.858790	DOWN
COL5A3	1.065334	4.483075	6.862145	3.06E-11	1.53E-07	15.141900	UP
KLRK1	-1.042080	-1.680550	-6.897570	2.45E-11	1.53E-07	14.944580	DOWN
KANK4	2.042531	-1.141330	6.815258	4.08E-11	1.63E-07	14.494770	UP
SHANK1	1.000385	-2.117020	6.778856	5.10E-11	1.70E-07	14.266560	UP
AQP9	1.446889	0.996351	6.639111	1.19E-10	2.98E-07	13.616160	UP
RFX8	1.105281	-1.531310	6.480035	3.08E-10	5.61E-07	12.629680	UP
MRO	1.219407	-1.604540	6.386617	5.35E-10	7.64E-07	12.125270	UP
APCDD1L	1.810332	-0.166960	6.310014	8.36E-10	9.83E-07	11.757560	UP
CD96	-1.040970	3.114405	-6.227440	1.35E-09	1.35E-06	11.512000	DOWN
OLFML2B	1.052800	4.365633	6.195919	1.61E-09	1.43E-06	11.343780	UP
LOX	1.055099	4.075536	6.192347	1.65E-09	1.43E-06	11.330860	UP
GXYLT2	1.372849	1.143017	6.183920	1.73E-09	1.44E-06	11.153180	UP
MCEMP1	1.188455	-1.582020	6.066237	3.37E-09	2.41E-06	10.443090	UP
TRIM31	-2.063130	2.625449	-5.961580	6.06E-09	3.67E-06	10.078170	DOWN
BCL2L14	-1.043860	1.195518	-5.962400	6.03E-09	3.67E-06	10.000840	DOWN
SIDT1	-1.033460	3.031041	-5.894390	8.79E-09	4.88E-06	9.741697	DOWN
ADAMTS12	1.229204	3.108628	5.879483	9.54E-09	4.95E-06	9.665697	UP
COL5A1	1.124697	7.530682	5.881197	9.45E-09	4.95E-06	9.557493	UP
SIRPG	-1.176660	0.455409	-5.860210	1.06E-08	5.18E-06	9.445412	DOWN
FAP	1.318922	2.934268	5.810812	1.39E-08	6.04E-06	9.308486	UP
SOX11	1.211480	-1.134280	5.836070	1.21E-08	5.50E-06	9.282945	UP
TGFBI	1.125431	7.143558	5.820502	1.32E-08	5.85E-06	9.241711	UP
POSTN	1.606819	6.352399	5.752116	1.91E-08	7.96E-06	8.903434	UP
RP11-863P13.3	1.261080	-1.406810	5.755573	1.88E-08	7.96E-06	8.880088	UP
TM4SF19	1.510747	-1.538310	5.727437	2.18E-08	8.73E-06	8.740387	UP
COL1A1	1.130808	10.913750	5.711120	2.38E-08	9.16E-06	8.659917	UP
RPLP0P2	1.084015	1.066891	5.696645	2.58E-08	9.71E-06	8.654919	UP
AC007750.5	1.035479	-2.382300	5.669416	2.98E-08	1.05E-05	8.448236	UP
ATP6V0D2	1.100900	-1.983740	5.503217	7.18E-08	1.97E-05	7.652699	UP
SCML4	-1.087250	-1.301690	-5.495600	7.47E-08	2.01E-05	7.622787	DOWN
COL1A2	1.048325	10.188270	5.493456	7.56E-08	2.01E-05	7.551791	UP
GLIS1	1.016775	-0.664570	5.462373	8.88E-08	2.34E-05	7.472662	UP
MMP9	1.467265	3.996145	5.444731	9.73E-08	2.49E-05	7.460258	UP
NGF	1.072695	-1.054970	5.454436	9.26E-08	2.40E-05	7.430413	UP
SPHK1	1.029125	4.334253	5.430783	1.05E-07	2.65E-05	7.370437	UP
FN1	1.199526	9.859929	5.419577	1.11E-07	2.74E-05	7.184263	UP
TNFAIP6	1.198632	1.452502	5.388467	1.30E-07	2.99E-05	7.179757	UP
ADCYAP1R1	1.115195	-2.254770	5.392186	1.28E-07	2.99E-05	7.127955	UP
APCDD1L-DT	1.325731	-2.106820	5.378497	1.37E-07	3.04E-05	7.065297	UP
ALDH1L2	1.075484	1.985114	5.346840	1.61E-07	3.39E-05	6.998903	UP
PLEKHG7	-1.209590	-1.616870	-5.337280	1.69E-07	3.45E-05	6.877589	DOWN
PLPP4	1.511714	0.325020	5.314792	1.90E-07	3.70E-05	6.802641	UP
ARSI	1.347362	1.717256	5.275471	2.31E-07	4.28E-05	6.657180	UP
GFPT2	1.390783	2.441277	5.265394	2.44E-07	4.43E-05	6.624135	UP
GPR1	1.276787	-0.734030	5.242341	2.74E-07	4.76E-05	6.449173	UP
CD109	1.116195	4.286468	5.235372	2.83E-07	4.76E-05	6.429603	UP
SLAMF9	1.133868	-2.184410	5.238676	2.79E-07	4.76E-05	6.420566	UP
COL6A3	1.003565	8.314517	5.226605	2.96E-07	4.85E-05	6.247512	UP
DDN	1.028646	-1.329790	5.187373	3.60E-07	5.58E-05	6.193463	UP
ADAMTS2	1.012568	4.628327	5.185067	3.64E-07	5.58E-05	6.167118	UP
TRAT1	-1.125820	-1.788230	-5.155870	4.21E-07	6.15E-05	6.048333	DOWN
CHST6	1.079384	1.053525	5.124272	4.93E-07	6.70E-05	5.945541	UP
IGSF21	1.013087	-0.190670	5.112810	5.21E-07	6.95E-05	5.869403	UP
UBD	-1.537310	0.917643	-5.086250	5.94E-07	7.64E-05	5.773166	DOWN
FNDC1	1.561474	2.377986	5.078308	6.18E-07	7.73E-05	5.759771	UP
FER1L4	-1.439590	6.430316	-5.113160	5.21E-07	6.95E-05	5.737915	DOWN
COL3A1	1.024116	10.077160	5.116326	5.12E-07	6.92E-05	5.719375	UP
CTHRC1	1.079193	4.849135	5.087088	5.92E-07	7.64E-05	5.692684	UP
IL9R	-1.095050	0.385362	-4.968760	1.05E-06	0.00011	5.240299	DOWN
RGS4	1.044460	1.318417	4.961968	1.09E-06	0.00011	5.226354	UP
OR2I1P	-1.463270	0.377064	-4.923390	1.31E-06	0.00013	5.043311	DOWN
COL10A1	1.735684	2.332818	4.917330	1.35E-06	0.00013	5.038258	UP
BCAT1	1.066768	4.355067	4.900837	1.46E-06	0.00014	4.876653	UP
CDA	1.024649	1.875659	4.875069	1.65E-06	0.00015	4.852061	UP
BICC1	1.030122	2.417180	4.873815	1.66E-06	0.00015	4.846246	UP
IL11	1.026015	1.339438	4.872633	1.67E-06	0.00015	4.835941	UP
ATOH8	-1.175980	2.007880	-4.846330	1.89E-06	0.00016	4.727478	DOWN
HMGA2	1.827664	0.190652	4.842575	1.92E-06	0.00017	4.692791	UP
TRGC2	-1.003470	-1.433260	-4.819180	2.14E-06	0.00018	4.578451	DOWN
FCGR3B	1.128418	-0.373830	4.809468	2.24E-06	0.00019	4.543775	UP
TCHH	1.182049	-0.567870	4.794080	2.41E-06	0.0002	4.477092	UP
EVA1A	1.049092	1.147154	4.747328	3.00E-06	0.00023	4.296546	UP
TENM3	1.333154	1.039663	4.743824	3.05E-06	0.00024	4.280945	UP
AHNAK2	1.403178	4.402885	4.755872	2.88E-06	0.00023	4.233062	UP
ASPN	1.058180	3.065845	4.726377	3.31E-06	0.00025	4.189637	UP
GPC6	1.106163	2.400580	4.702207	3.70E-06	0.00027	4.105045	UP
SPP1	1.129788	6.006959	4.748854	2.98E-06	0.00023	4.090777	UP
HTRA3	1.043908	5.058976	4.732754	3.21E-06	0.00024	4.075259	UP
FPR1	1.006921	1.725611	4.688535	3.94E-06	0.00028	4.051818	UP
RFLNA	1.232167	-0.101370	4.680285	4.09E-06	0.00029	4.003665	UP
CRTAC1	-1.820160	0.965313	-4.661230	4.46E-06	0.0003	3.934495	DOWN
DSC2	1.094913	4.897944	4.688897	3.93E-06	0.00028	3.896092	UP
KCNJ12	1.055319	-1.269270	4.649875	4.70E-06	0.00031	3.871375	UP
WNT11	1.196999	0.440641	4.633038	5.08E-06	0.00033	3.812410	UP
CYP4F12	-1.490920	3.266569	-4.615530	5.50E-06	0.00035	3.708361	DOWN
TREM1	1.052329	1.284111	4.600042	5.90E-06	0.00037	3.681888	UP
WSCD2	-1.457980	0.974231	-4.587790	6.23E-06	0.00038	3.630380	DOWN
MT1H	1.125404	-1.733140	4.588307	6.22E-06	0.00038	3.618043	UP
BTBD16	-1.842360	2.319848	-4.584230	6.33E-06	0.00038	3.609781	DOWN
FIBIN	1.155813	1.404852	4.569673	6.76E-06	0.0004	3.557268	UP
SHOX2	1.034906	-0.200990	4.546716	7.50E-06	0.00042	3.455211	UP
SORCS2	1.119009	1.286042	4.533575	7.95E-06	0.00044	3.409532	UP
KLHDC7A	-1.788250	2.777923	-4.538050	7.80E-06	0.00043	3.405910	DOWN
CDH2	1.004207	0.802186	4.513417	8.70E-06	0.00046	3.326136	UP
MT1G	1.013186	0.757514	4.504971	9.04E-06	0.00047	3.291847	UP
LRRC15	1.485039	1.862273	4.461906	1.09E-05	0.00053	3.116157	UP
PTPRN	1.087380	-1.115900	4.446432	1.17E-05	0.00056	3.050625	UP
GAS1	1.139113	2.421687	4.422065	1.30E-05	0.00061	2.944579	UP
CHI3L1	1.341528	4.195358	4.409610	1.38E-05	0.00063	2.783862	UP
FXYD3	-1.032450	8.637088	-4.416790	1.33E-05	0.00062	2.624327	DOWN
SBSN	1.702321	0.687232	4.333482	1.92E-05	0.0008	2.612043	UP
IGF2BP2	1.207508	3.278038	4.341633	1.85E-05	0.00078	2.580425	UP
MT1M	1.023934	-0.218360	4.316445	2.06E-05	0.00083	2.544516	UP
CXCL5	1.482159	-0.032330	4.291189	2.30E-05	0.00088	2.447669	UP
ADAMTS16	1.087869	0.376127	4.290548	2.30E-05	0.00088	2.445569	UP
SFRP2	1.783090	4.536242	4.325623	1.98E-05	0.00081	2.421433	UP
CPA4	1.377783	0.766505	4.272485	2.49E-05	0.00092	2.375823	UP
CTSE	-1.721350	1.782539	-4.248500	2.76E-05	0.00099	2.273768	DOWN
CYP4B1	-1.653020	5.298083	-4.295540	2.26E-05	0.00088	2.233463	DOWN
CYP4F29P	-1.349810	-0.313740	-4.232840	2.95E-05	0.00103	2.224330	DOWN
ACOXL	-1.203800	1.543386	-4.231960	2.96E-05	0.00103	2.214724	DOWN
PTGER3	1.010425	0.506798	4.216297	3.16E-05	0.00107	2.161626	UP
HTR1D	1.073736	-0.661660	4.181176	3.66E-05	0.00117	2.029147	UP
SNCG	-1.113220	7.275854	-4.257020	2.66E-05	0.00096	1.985972	DOWN
HAS1	1.119314	-1.160600	4.157452	4.04E-05	0.00126	1.940232	UP
PTHLH	1.197832	2.732664	4.168194	3.87E-05	0.00122	1.933820	UP
PACRG	-1.082780	-1.148660	-4.141070	4.33E-05	0.00131	1.879289	DOWN
SPRR1B	1.735026	1.820999	4.143041	4.29E-05	0.0013	1.870628	UP
PCSK9	1.243465	0.247156	4.126220	4.60E-05	0.00136	1.823641	UP
PLA2G2A	-1.402040	3.800965	-4.158330	4.03E-05	0.00125	1.818198	DOWN
TNNT1	1.198463	1.461371	4.096420	5.21E-05	0.00147	1.703646	UP
PI3	1.878765	2.284384	4.041985	6.51E-05	0.00172	1.477640	UP
COL11A1	1.316415	2.948739	4.047008	6.38E-05	0.00169	1.462312	UP
SYNDIG1	1.024218	-0.132850	4.014299	7.28E-05	0.00188	1.413961	UP
SLC44A4	-1.281270	4.304132	-4.014110	7.29E-05	0.00188	1.219740	DOWN
RP11- 510N19.5	-1.054760	1.640855	-3.953520	9.31E-05	0.00222	1.175609	DOWN
BCAS1	-1.374580	4.368733	-4.003450	7.61E-05	0.00195	1.174520	DOWN
ARL14	-1.118800	1.424985	-3.948120	9.51E-05	0.00226	1.160885	DOWN
ZNF114	1.031478	0.218503	3.938725	9.87E-05	0.00231	1.141337	UP
LGALS4	-1.296960	0.915877	-3.939360	9.85E-05	0.00231	1.137368	DOWN
GNG4	1.114596	0.876367	3.909349	0.00011	0.0025	1.031364	UP
SMIM22	-1.073010	4.711593	-3.959360	9.09E-05	0.00218	0.969334	DOWN
BLK	-1.027910	-1.779020	-3.883410	0.00012	0.00269	0.950270	DOWN
HPGD	-1.330640	5.831239	-3.976500	8.49E-05	0.0021	0.948738	DOWN
EREG	1.397041	1.038786	3.859063	0.00014	0.00289	0.850807	UP
BHMT	-1.759090	0.986506	-3.852950	0.00014	0.00294	0.828875	DOWN
SCNN1G	-1.406210	3.188227	-3.865040	0.00013	0.00285	0.776855	DOWN
CYP4F35P	-1.157100	-1.367500	-3.831890	0.00015	0.00312	0.770540	DOWN
MFAP5	1.329649	1.494187	3.832023	0.00015	0.00312	0.746596	UP
FOXA1	-1.184510	5.119461	-3.848550	0.00014	0.00298	0.525246	DOWN
CYP4F8	-1.841180	1.246215	-3.745090	0.00021	0.00387	0.449189	DOWN
BMP5	-1.141370	-1.054500	-3.731220	0.00022	0.00402	0.425791	DOWN
CALB2	1.092114	0.029127	3.717678	0.00023	0.00412	0.375437	UP
DPT	1.268705	1.091875	3.709977	0.00024	0.00422	0.335047	UP
CYP4F11	-1.099920	2.692770	-3.723700	0.00023	0.00409	0.314964	DOWN
IGHD	-1.326770	-0.038390	-3.683560	0.00027	0.00451	0.260683	DOWN
CXCL13	-1.224080	2.281208	-3.692910	0.00026	0.00442	0.234236	DOWN
KRT1	1.502345	-0.569380	3.664419	0.00029	0.00474	0.199952	UP
UPK3A	-1.662930	2.850760	-3.669290	0.00028	0.00469	0.116654	DOWN
AZGP1	-1.114170	0.505928	-3.583540	0.00039	0.00582	-0.075750	DOWN
SCEL	1.308267	0.591569	3.563183	0.00042	0.00612	-0.143690	UP
KLK10	1.424091	-0.176860	3.551144	0.00044	0.0063	-0.174090	UP
FABP6	-1.082620	2.021978	-3.550010	0.00044	0.0063	-0.230770	DOWN
SCNN1B	-1.174720	4.572382	-3.616710	0.00034	0.00537	-0.238470	DOWN
PTPRR	-1.074670	1.802206	-3.531570	0.00047	0.00658	-0.280520	DOWN
SLC14A1	-1.403320	4.003877	-3.580640	0.00039	0.00586	-0.294330	DOWN
FAM3B	-1.310420	3.669774	-3.565280	0.00041	0.00611	-0.311930	DOWN
GPX2	-1.450250	5.918965	-3.626500	0.00033	0.00522	-0.315670	DOWN
MARCO	1.033158	0.572763	3.453083	0.00062	0.00806	-0.496050	UP
GREM1	1.197612	4.247884	3.521688	0.00049	0.00671	-0.523980	UP
LINC02888	-1.340250	0.699407	-3.437090	0.00066	0.00836	-0.550290	DOWN
ADGRF1	-1.161070	4.206133	-3.509500	0.00051	0.00693	-0.558280	DOWN
GGT6	-1.074030	4.842966	-3.528110	0.00047	0.00662	-0.570200	DOWN
CYP4F23P	-1.291470	0.771543	-3.429160	0.00068	0.00852	-0.576660	DOWN
MS4A1	-1.125900	-0.756330	-3.422710	0.00069	0.00858	-0.577810	DOWN
CXCL6	1.028334	0.567302	3.371193	0.00083	0.00969	-0.751850	UP
DSG3	1.707794	1.415782	3.354856	0.00088	0.01008	-0.828200	UP
HNF1B	-1.198150	1.760429	-3.275610	0.00116	0.01211	-1.085170	DOWN
ATP1A4	-1.209850	0.954816	-3.264450	0.0012	0.01246	-1.087890	DOWN
CAPN8	-1.191680	1.459386	-3.223650	0.00138	0.01368	-1.227950	DOWN
MROH2A	-1.061710	-0.639530	-3.197120	0.00151	0.01453	-1.260750	DOWN
TSPAN8	-1.061390	-0.178780	-3.154650	0.00175	0.01603	-1.388910	DOWN
VSIG2	-1.122950	5.093133	-3.235920	0.00133	0.01325	-1.538070	DOWN
IGF2BP3	1.067470	0.236196	3.084983	0.0022	0.0187	-1.594740	UP
PM20D1	-1.449940	1.361915	-3.086030	0.00219	0.01867	-1.627450	DOWN
PLA2G2F	-1.347330	4.061319	-3.145670	0.0018	0.01638	-1.687810	DOWN
SNX31	-1.361950	3.218136	-3.099070	0.0021	0.01818	-1.727410	DOWN
CSF3	1.039187	-0.470350	2.991406	0.00297	0.02294	-1.846330	UP
S100A8	1.173305	5.592384	3.125185	0.00192	0.01715	-1.918870	UP
KRT6A	1.665864	4.945746	3.082547	0.00221	0.01879	-1.976490	UP
SERPINB2	1.149847	0.533881	2.907731	0.00387	0.02744	-2.091590	UP
SFRP4	1.202461	3.351567	2.951017	0.00338	0.02498	-2.165650	UP
HMGCS2	-1.571180	3.535442	-2.938420	0.00352	0.02567	-2.221430	DOWN
SHH	-1.278520	0.671597	-2.859590	0.00449	0.03046	-2.225590	DOWN
ANXA10	-1.361430	0.233399	-2.837090	0.00482	0.03192	-2.273900	DOWN
DHRS2	-1.279700	7.110129	-2.998770	0.0029	0.02258	-2.357530	DOWN
UCA1	-1.110140	4.331877	-2.904120	0.00392	0.02768	-2.423930	DOWN
CLCA4	-1.368160	1.800711	-2.798560	0.00542	0.0343	-2.439280	DOWN
TMPRSS2	-1.039540	4.586831	-2.847560	0.00466	0.03125	-2.614410	DOWN
PSCA	-1.245210	7.534588	-2.892610	0.00406	0.02833	-2.667400	DOWN
SPINK1	-1.480600	4.590088	-2.776450	0.00579	0.03601	-2.798840	DOWN
FGFBP1	1.122102	1.720014	2.635276	0.00878	0.04803	-2.846580	UP

According to the standard of adj.P.Val <0.05& abs(logFC) >1, we obtained a total of 194 differential genes through the "limma" package, including 117 up-regulated genes and 77 down-regulated genes.

https://dx.doi.org/10.21037/tcr-22-2255

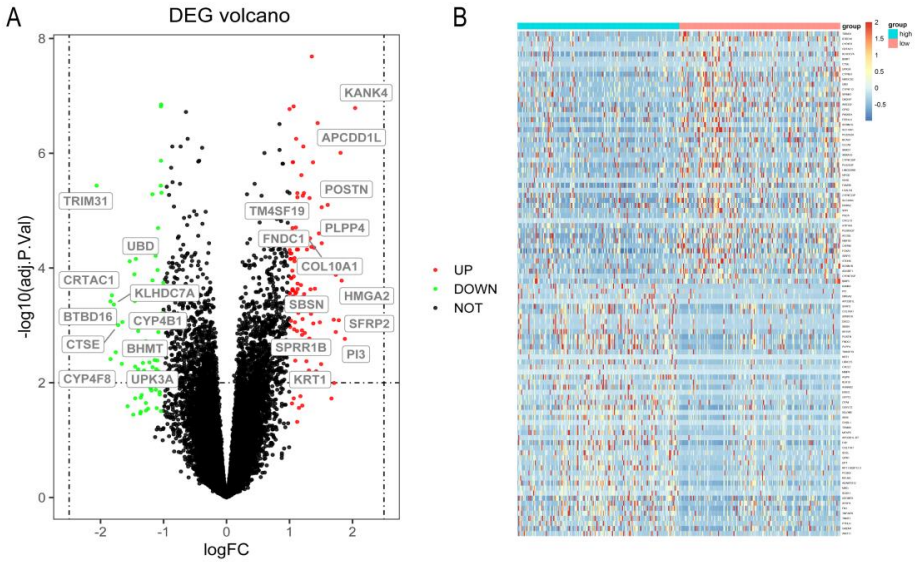

Figure S3 Volcano plot and heatmap of 194 differential genes between high-risk group and low-risk group. (A) In the volcano plot, the differential genes that met adj.P.Val <0.01 & abs(logFC) >1.5 would be marked with gene symbols. (B) The heatmap presents the top 50 up-regulated genes and the top 50 down-regulated genes.

https://dx.doi.org/10.21037/tcr-22-2255